IOP Publishing Measurement Science and Technology
Meas. Sci. Technol. **31** (2020) 055302 (8pp) https://doi.org/10.1088/1361-6501/ab6916

Improvement of the signal-to-noise ratio of the constant-temperature hot-wire anemometer using the transfer function

Ayumu Inasawa, Shohei Takagi and Masahito Asai

Department of Aeronautics and Astronautics, Tokyo Metropolitan University 6-6 Asahigaoka, Hino, Tokyo 191-0065, Japan

E-mail: ainasawa@tmu.ac.jp, pantaka@tmu.ac.jp and masai@tmu.ac.jp

Received 2 October 2019, revised 20 December 2019
Accepted for publication 8 January 2020
Published 5 March 2020

Abstract

In the present paper, a compact low-noise constant-temperature hot-wire anemometer (CTA) was developed to improve the signal-to-noise (S/N) ratio in hot-wire measurements. The CTA circuit was small enough to be attached to the support stem directly, which minimized the reactance of the sensor cable, maximized the electromagnetic shielding effect and simplified the circuit's transfer function. White noise as well as a square wave were used to examine the dynamic responses of the CTA in detail. Three parameters in the transfer function were successfully determined by the square-wave test. The transfer function with experimentally determined parameters was found to describe the CTA responses quite well over the wide frequency range, from 1 Hz to 250 kHz. It was demonstrated for residual free-stream turbulence in a wind tunnel that the established transfer function allowed the separation of electric noise from the measured data, improving the S/N ratio in the power spectrum of the velocity fluctuations.

Keywords: constant temperature hot-wire anemometer, transfer function, compact low-noise CTA, improving signal-to-noise ratio

(Some figures may appear in colour only in the online journal)

1. Introduction

Hot-wire anemometry (HWA) [1, 2] is one of the popular techniques for measuring time-dependent fluid flows. The most notable advantage of HWA is the capability of accurately measuring velocity fluctuations over a wide frequency range, even if the fluctuations are extremely weak (for instance, of the order of only 0.01% of the mean velocity), compared to other velocimetries such as particle image velocimetry (PIV) and laser Doppler velocimetry (LDV); thus, HWA still holds a predominant position in fluid dynamics experiments, especially on flow instability and transition to turbulence [3–6] and wall turbulence structures [7–10]. This paper focuses on the constant-temperature hot-wire anemometer (CTA), because the CTA system has an advantage in that it is free from burnout damage to the hot-wire sensor, irrespective of the magnitude of the fluid velocity, compared to the constant-current anemometer. It is well known that regarding the signal-to-noise (S/N) ratio, there is no appreciable difference between the constant-current mode and the constant-temperature mode of HWA under identical environmental conditions [11].

Recently, many researchers have studied how the spatial/temporal resolution of hot-wire sensors affects the measurements of velocity fluctuations in turbulent flows. The resolution problem of HWA is, needless to say, one of the most important issues in experiments on wall turbulence [12–14] and on grid turbulence [15] at high Reynolds numbers. However, the achievement of a higher S/N ratio over a wide frequency range is also essential to capture flow properties accurately. This becomes rather critical in the measurement of turbulence dissipation at high Reynolds numbers. To this end, the inherent electric noise of HWA has to be reduced as much as possible. There are three possible noise sources in the CTA system. The first is electric noise coming from the power line. The second is inherent feedback noise of the servo amplifier,

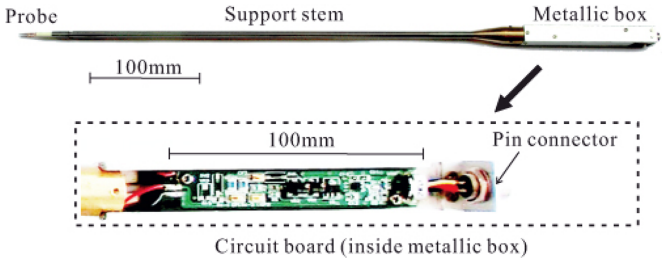

Figure 1. The newly designed CTA system. The CTA circuit board is installed in a metallic box.

which plays a major role in the CTA. The last is the so-called spiky noise electromagnetically induced on the cable connecting a hot-wire sensor and the CTA bridge, which may be ascribed to the power lines or other electric/electronic devices. The first noise can be reduced significantly if the system runs on batteries. As for the second, the best solution is to employ the lowest-noise operational amplifier available. Electromagnetic shielding of the sensor cable with conductive media is known to be effective for reducing the third noise.

In addition, it is desirable to shorten the sensor cable as much as possible, demonstrating another advantage of the dynamic response of the CTA bridge to velocity fluctuations. When the reactance (capacitance and/or inductance) of the sensor cable connecting the hot-wire and the servo amplifier in the CTA bridge is not small, the transfer function of the system's response to velocity fluctuations generally constitutes a fifth-order equation [16]. If the cable reactance was reduced to a negligible level, the behavior of the CTA system would follow a third-order [17, 18] or a second-order equation [19], depending on the servo-amplifier configuration used. When a single-stage amplifier with a first-order frequency response is used, the three parameters in the second-order transfer function could be determined experimentally by introducing external electric signals, such as sinusoidal or square waves and white noise. We could therefore expand the dynamic response range of the CTA system using the transfer function. Furthermore, it would be possible to eliminate the inherent electric noise attributed to the feedback system of the CTA bridge.

In the present study, we aim to improve the S/N ratio in CTA measurements, developing a tiny CTA system with a sufficiently short sensor cable. The CTA circuit board installed in a metallic box was attached at the end of the hot-wire support stem directly; thus, the whole system could be immersed in the flow. The dynamic responses of the developed CTA were investigated in detail and compared with the theoretical transfer function. Low-noise performance of the newly developed CTA and its improvement using the established transfer function are presented.

2. Experimental setup

2.1. CTA and data acquisition system

A single hot-wire sensor was made of tungsten, with a diameter (d) of 5 μm and length (l) of 1 mm; thus l/d was 200. With the exception of the sensing portion, the wire was copper-plated with a thickness of about 60 μm, and soldered on the two prong tips 3 mm apart. Figure 1 shows a photograph of the newly designed CTA system. A small CTA circuit board, consisting of a prevalent CTA bridge [19, 20], was installed in a metallic box with a cross-section of 14×14 mm^2 and length of 120 mm. Thus, the length of the sensor cable passing through the support stem was only 450 mm, and the reactance was negligibly small, as shown later.

The CTA box had a pin connector for an output signal, a DC power supply from lead acid batteries and an external signal input. In the electric test, a square-wave signal with a 1 kHz frequency from a function generator (NF Corp. WF1974), or a white-noise signal generated digitally using MATLAB and converted by a 16-bit digital-to-analog converter (NI USB6259) at a sampling rate of 1 MHz, was introduced into the CTA bridge. The CTA system, mounted on the traversing mechanism, was set horizontally in the middle of the wind-tunnel test section.

The CTA output, via a fourth-order anti-aliasing filter with a roll-off frequency of 215 kHz, was acquired through an A/D converter with a resolution of 24 bits at a sampling rate of 500 kHz (Analog Devices DC2390A).

2.2. Wind tunnel

The CTA system was tested in an open-jet type low-speed wind tunnel with a cross section of 600×300 mm^2. The free-stream velocity U_∞, which was measured using a pitot tube, was varied continuously over a range of 1–35 m s^{-1}. The residual turbulence level over the frequency range of 1 Hz to 2 kHz was less than 0.1% of U_∞ at $U_\infty = 20$ m s^{-1}. The CTA bridge output was digitally linearized using fourth-order polynomials in a PC.

3. Theory for CTA frequency response

3.1. Static characteristics of the CTA bridge

Figure 2 shows a schematic of the CTA bridge. The basic circuit consists of a Wheatstone bridge and a servo amplifier of gain A with a zero-adjustment trimpot. An input terminal for the external signal e_t at the upper arm of the hot-wire sensor is equipped to investigate the dynamic-response characteristics of the CTA system.

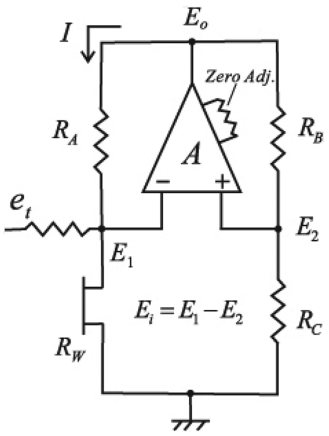

Figure 2. The simplified CTA bridge circuit with a damping trimmer and an external-signal terminal.

When the hot-wire of resistance, R_W, heated by current, I, in the flow of velocity, U, is in the thermal equilibrium state, the following equation holds:

$$R_W = \frac{R_A R_C}{R_B} + \Delta R_W = \tilde{R}_W + \Delta R_W \tag{1}$$

$$\Delta R_W = -\frac{(R_A + R_W)(R_B + R_C)}{A R_B}\left(1 + A\frac{\Delta E}{E_o}\right) \tag{2}$$

$$I = \frac{E_o}{R_A + R_W} = -\frac{A(E_i + \Delta E)}{R_A + R_W} \tag{3}$$

where ΔR_W is called the imbalance resistance that can be tuned by ΔE using a zero-adjustment trimmer of the amplifier. Equations (1)–(3) imply that the hot-wire balances with a bias of ΔR_W shifted from the resistance in the ideal equilibrium state $\tilde{R}_W$. The imbalance resistance is very small in the present configuration ($A \gg 1$ and $A(\Delta E/E_o) \sim O(1)$). The adjustment of ΔE is carried out to optimize the frequency response of the CTA circuit to the velocity fluctuations, especially around a resonance (roll-off) frequency of the circuit, as will be explained later in sections 3.2 and 3.3.

In the present study, the resistance values in the bridge were $R_A = 20\ \Omega$, $R_B = 200\ \Omega$, and $R_C = 56\ \Omega$, giving the bridge ratio of 10 and the overheat ratio of 0.55 for the hot-wire sensor mentioned in section 2.1. A very low-noise operation amplifier (Analog Devices LT6201) was employed as a servo amplifier.

3.2. Dynamic response of the CTA bridge

Dynamic response to a sinusoidal perturbation ($\propto \exp(j\omega t)$) in the velocity fluctuation u and/or external electric signal e_t has been analyzed in several studies (e.g. Wood [16], Freymuth [17, 18], Weidman and Browand [19] and Itsweire and Helland [20]; also see review books by Perry [1] and Bruun [2]). In the present study, a single-stage amplifier with a first-order frequency response

$$e_o = -\frac{A e_i}{1 + j\omega\mu} \qquad (j = \sqrt{-1}) \tag{4}$$

is employed, where e_i and e_o ($= (\tilde{R}_W + R_A)i$) are variations in the input and output voltage, respectively, and ω and μ, respectively, are the angular frequency and time constant of the servo amplifier. Here, e_i includes electric noise e_t and a contribution from the imbalance voltage $\Delta R_W i$:

$$e_i = I r_W + \Delta R_W i + e_t \tag{5}$$

where r_W and i are the variations in resistance of the hot-wire sensor and heating current, respectively.

The heat balance equation of a hot wire under constant fluid temperature T_e yield the following equation:

$$r_W(1 + j\omega M) = \left(\frac{\partial R_W}{\partial I}\right)_U i + \left(\frac{\partial R_W}{\partial U}\right)_I u \tag{6}$$

Here, the time constant of the hot wire M is given by

$$M = \frac{C_W a_W}{\alpha R_e I^2} \tag{7}$$

where C_W, a_W, R_e and α are the sensor heat capacity, the overheat ratio of the hot wire, the resistance of the hot-wire sensor at T_e and the temperature coefficient of resistance for the sensor material, respectively. From these equations, the transfer function for the output voltage of the hot wire $e_o(t)$ in the constant-temperature mode can be derived as

$$\begin{aligned} e_o(t) &= \frac{K(\partial E_o/\partial U)_{R_W} u - A(1 + j\omega M) e_t}{K + K\delta(1 + j\omega M) + (1 + j\omega M)(1 + j\omega\mu)} \\ &= \frac{K(\partial E_o/\partial U)_{R_W} u - A(1 + j\omega M) e_t}{(K + K\delta + 1)\left[1 + 2\zeta(j\omega/\omega_r) + (j\omega/\omega_r)^2\right]} \end{aligned} \tag{8}$$

with

$$\omega_r^2 = \frac{K + K\delta + 1}{\mu M} \tag{9}$$

$$2\zeta = \frac{1 + K\delta + \mu/M}{\mu\omega_r} \tag{10}$$

Here, the constants $\delta = (\Delta R_W/\tilde{I})/(\partial R_W/\partial I)_U$ and $K = A\tilde{I}(\partial R_W/\partial I)_U/(\tilde{R}_W + R_A)$ are the DC imbalance parameter and DC feedback-loop rate, respectively, and the tilde denotes the values in the ideal (non-bias) equilibrium state. Here, $(\partial E_o/\partial U)_{R_W}$, which is equal to $-(\tilde{R}_W + R_A)(\partial R_W/\partial U)_I/(\partial R_W/\partial I)_U$ in the constant-temperature mode, denotes the velocity sensitivity of the CTA. If no external signal is supplied, that is, $e_t = 0$, it turns out that equation (8) is a low-pass filter (with two poles) to the velocity fluctuation u; in other words, the parameters ζ and ω_r correspond to the damping coefficient and resonance/roll-off frequency of the circuit's response to the velocity fluctuation, respectively. Equation (8) includes three unknown parameters, ω_r, ζ, and M, which depend on both the flow velocity and configuration of the hot-wire sensor. These parameters are determined by investigating the response of the CTA bridge to the square-wave signal in the next section.

3.3. Response of the CTA bridge to square-wave input

When the square-wave current (as the input signal e_t) is injected into the CTA bridge, the servo amplifier begins to return the bridge to balance. In this case, assuming that the velocity fluctuation u is negligibly small compared to the input signal e_t, such as in low free-stream turbulence environments, the transfer function is approximately derived by performing the Laplace transformation of the perturbation equation with the Heaviside step function (unit step input), that is, $e_t = 0$ V for $t < 0$ s and $e_t = 1$ V for $t \geq 0$ s. The Laplace transform of the output voltage $\hat{e}_o(s)$ is written as

$$\hat{e}_o(s) = -\left[\frac{1+sM}{(1+s\mu)(1+sM)+K\delta(1+sM)+K}\right]\frac{1}{s} = -\frac{1}{\mu}\left[\frac{s+1/M}{s(s^2+2\zeta\omega_r s+\omega_r^2)}\right] \tag{11}$$

and the inverse Laplace transform of equation (11) gives the response to the step function as follows:

$$e_o(t) = -\frac{T_r^2}{\mu M}\left[1+\mathrm{e}^{-\frac{\zeta t}{T_r}}\left(-\cos\frac{t\sqrt{1-\zeta^2}}{T_r}-\frac{\zeta}{\sqrt{1-\zeta^2}}\times\sin\frac{t\sqrt{1-\zeta^2}}{T_r}+\frac{M}{T_r}\frac{1}{\sqrt{1-\zeta^2}}\sin\frac{t\sqrt{1-\zeta^2}}{T_r}\right)\right] \tag{12}$$

where $T_r = 1/\omega_r$.

The coefficient M/T_r of the last term on the right-hand side in equation (12), which is due to the feedback effect of the servo amplifier, takes a value of 45–50 in the present experiment, much larger than the other three terms. Therefore, generally in past research only this term has been used to check and adjust the CTA responses [2]. In the present study, all the terms in equation (12) were considered, and all parameters depending on the flow velocity U (i.e. ζ, ω_r and M) were determined by a curve-fitting method. Here, it should be noted that the damping coefficient ζ should be positive in the constant-temperature mode because the output voltage of the CTA circuit diverges in time to the velocity fluctuation u for $\zeta < 0$, as seen from equation (12). The value of ζ can be adjusted by tuning ΔE, using the zero-adjustment trimpot of the servo amplifier (see equations (2) and (10)).

4. Results and comparison with theory

4.1. Bridge response to square-wave input

Before investigating the bridge responses in detail, the damping of the system to the square-wave input was set by tuning the zero adjustment of the servo amplifier in the bridge circuit (see figure 2), at a constant velocity of $U = 20$ m s^{-1}. The adjustments were made manually such that the response waveform to the square-wave input became the optimum shape [2] (neither overdamped nor underdamped) on the oscilloscope screen; that is, the damping coefficient $\zeta \approx 0.7$. Then, the transient waveform of the CTA bridge was acquired and compared to the theoretical response given by equation (12).

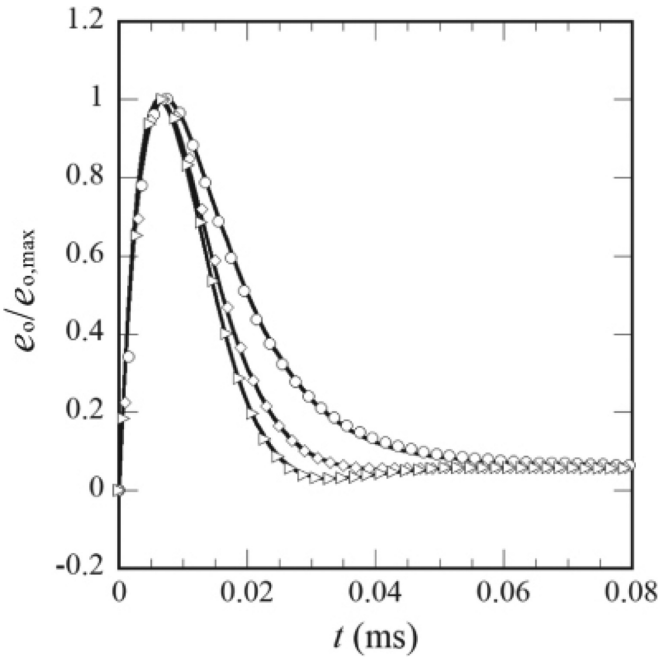

Figure 3. Transient responses to the square-wave input, compared with the theoretical curve (solid lines) for different flow velocities: ○, $U = 4$ m s^{-1}; ◇, $U = 12$ m s^{-1}; ▷, $U = 20$ m s^{-1}. The damping parameter $\zeta = 0.75$ at $U = 20$ m s^{-1}.

Figure 3 compares the response waveforms obtained at $U = 4$, 12 and 20 m s^{-1} to the theoretical curves given by equation (12) with the best-fitted parameters. Here, each output signal was normalized to a peak value of its waveform. The comparison shows that the theoretical model reproduced the actual response of the CTA well. Here, the damping parameter was determined to be $\zeta = 0.75$ at $U = 20$ m s^{-1}. The agreement suggested that reactance of the present 450 mm long sensor cable did not affect the dynamic response of the CTA system over the frequency range up to 250 kHz. Note that the thermal time constant M of the sensor, as well as the resonant frequency of the CTA ω_r, are essential to represent the response for $t/T_r \gg 1$. Similar square-wave tests were repeated at other velocities. Three parameters obtained from these tests are plotted in figure 4. All the parameters are dependent on the velocity U. That is, ζ and M decreased with increasing U, which indicates that the CTA system became underdamped as U increased, while ω_r increased with increasing U, in accordance with equation (9).

4.2. Bridge response to white-noise input

To confirm the validity of the three parameters determined by the present curve-fitting method, we supplied a white-noise signal to the bridge, instead of the square wave, to examine the response of the CTA system over a wide frequency range at $U = 20$ m s^{-1}. Figure 5 illustrates the power spectrum of the CTA output, where the damping coefficient ζ was 0.75, the same as in figure 3. Spectral components in the frequency range lower

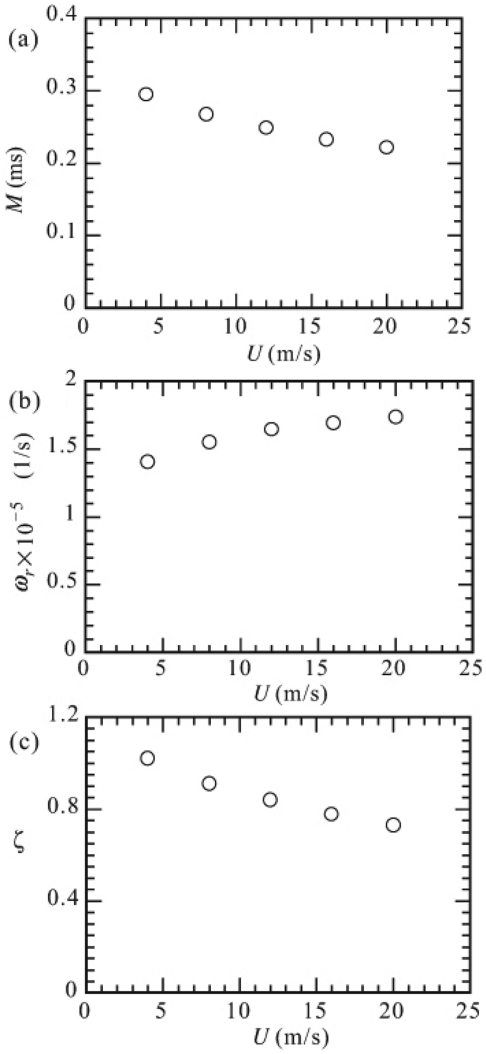

Figure 4. Velocity dependence of three parameters (a) M, (b) ω_r, (c) ζ. The damping parameter ζ is set at $U = 20$ m s^{-1}.

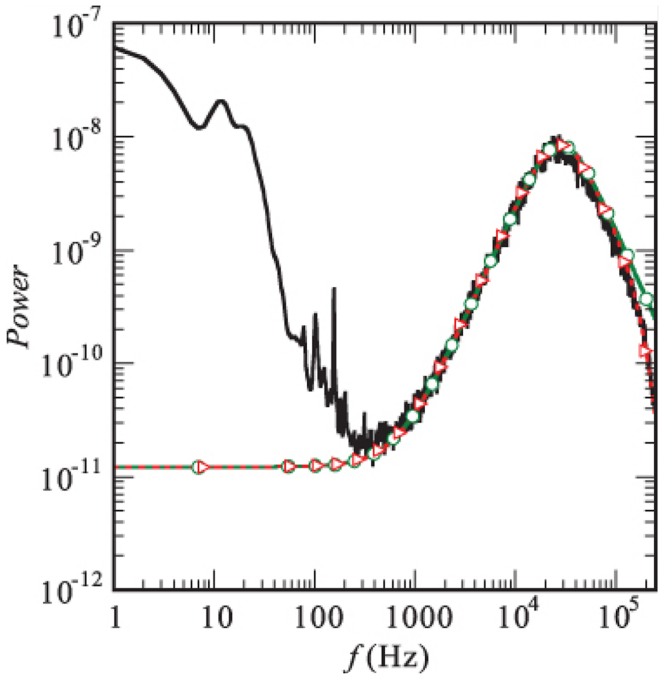

Figure 5. The power spectrum of the CTA bridge output forced by white noise for $\zeta = 0.75$ and $U = 20$ m s^{-1}. The power is displayed in terms of the streamwise velocity fluctuation normalized with the free-stream velocity U. Black line, actual response; ○, equation (8) with $e_t = 1$ ($u = 0$); ▷, equation (8) with an anti-aliasing filter.

than 300 Hz corresponded to the residual turbulence of the wind tunnel, while a large bump in the frequency range beyond 300 Hz was due to the injection of white noise. The green curve represents the square of the magnitude of the output voltage given by equation (8) with $u = 0$, where the three parameters were as in figure 4; the amplitude factor was determined in such a way that the bump peak matched the measurement. Taking the effect of the anti-aliasing filter into account, we concluded that the experimental result was perfectly consistent with the theoretical models (red curve), which also revealed that the inherent response characteristics of the CTA system were well represented by equation (8). Here, it should be emphasized that the white-noise input yielded the ratio of the peak value of the bump to the magnitude of the spectral components lower than 300 Hz. Let us focus on the red curve in figure 5. The ratio of the peak value of the bump to the magnitude of fluctuations lower than 100 Hz was approximately 10^3 in terms of the power. On the other hand, equation (8) gives the ratio of the peak value at the resonant frequency to the flat level in the lower frequency range as $M/(\sqrt{2}T_r)$ when $\zeta = 0.7$. Taking the magnitude of the power spectrum in figure 5 into account, this leads to a value of $(M/(\sqrt{2}T_r))^2 = 10^3$, giving $M/T_r \approx 45$, which coincides with that obtained from figure 4. This means that the thermal time constant of the hot wire is virtually reduced to 1/45 due to the feedback effect in the CTA, expanding the available frequency range.

The frequency responses of the CTA bridge with two different damping coefficients $\zeta = 0.96$ and 0.61 at $U = 20$ m s^{-1} were examined in a similar way, and the results are presented in figure 6, again confirming the validity of the curve-fitting method and equation (8). The consistency between the experiment and the theoretical model no doubt results from the fact that the reactance of the sensor cable was negligibly small, at least to the frequency of 250 kHz in the present CTA system.

In general, the resonant frequency ω_r serves as a kind of yardstick for the upper limit frequency of the CTA bridge, which corresponds to the roll-off frequency of the low-pass filter (with two poles), as already mentioned. However, since the theoretical model with three parameters determined from the square-wave test was found to describe the frequency response of the CTA accurately, we may now remove electrical effects ideally in the frequency range over which equation (8) is applicable. That is, both the phase and amplitude of the CTA bridge output can be compensated up to 250 kHz in the present system, using the denominator of equation (8) in the complex domain. It is worth pointing out that as long as the magnitude of the ?cins?external white-noise signal to the CTA bridge was kept constant, the magnitudes of the spectral components in the lower frequency range ($f \leq 100$ Hz) were independent of the damping coefficient ζ, while the magnitude of the bump's peak ($f = 20$–30 kHz) depended on ζ, as shown in

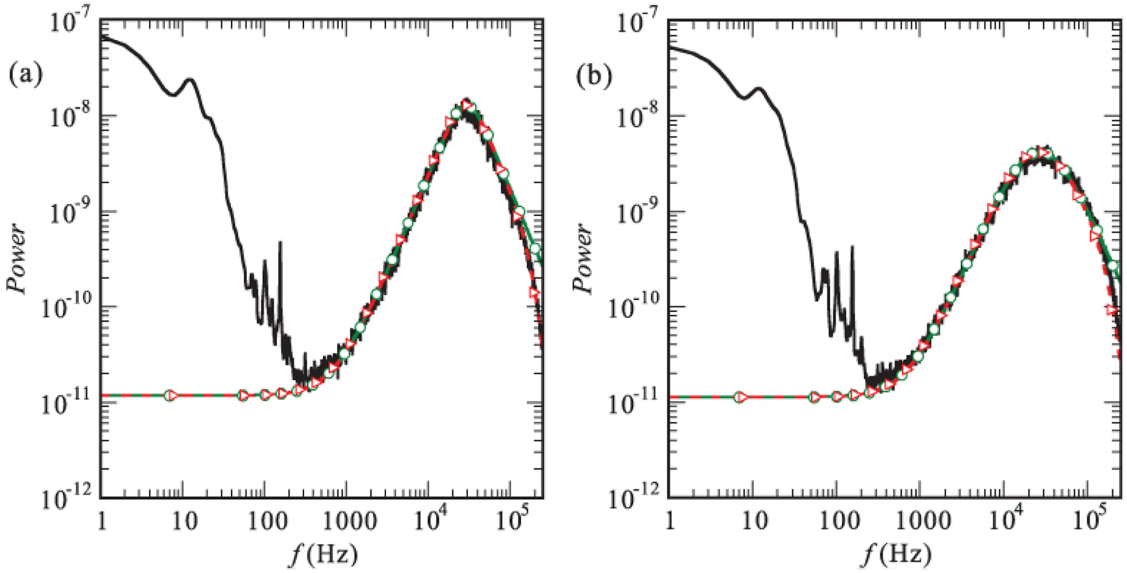

Figure 6. The results for (a) $\zeta = 0.61$ (underdamped) and (b) $\zeta = 0.96$ (overdamped) at $U = 20$ m s^{-1}. The colors are the same as those in figure 5.

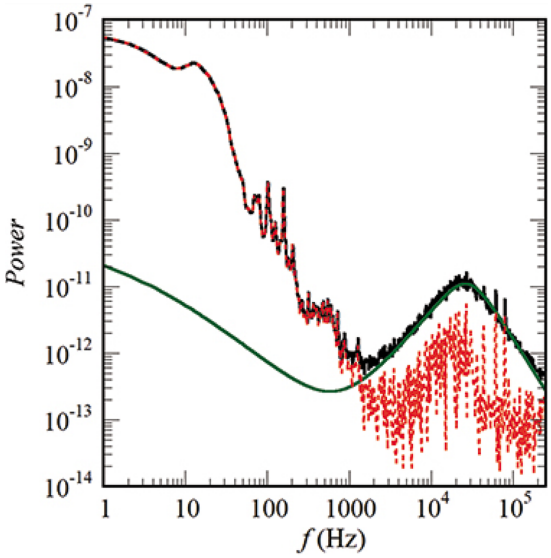

Figure 7. Power spectra with no external signal input and the estimated CTA noise for $\zeta = 0.75$ and $U = 20$ m s^{-1}. The black line represents the measured spectrum and the green line the electric noise evaluated. The estimated turbulence is depicted by the red broken line.

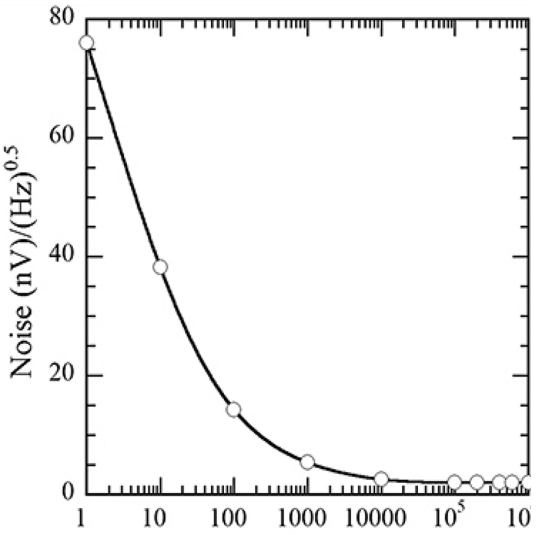

Figure 8. Spectrum density of the servo-amplifier input noise. The open circles are from the datasheet [21]. The solid line is the fitting curve of the ninth-order polynomial.

figures 5 and 6. This feature is useful for evaluating the inherent electric noise in the feedback loop of the CTA bridge as well, as we explain in the next section.

4.3. Electric noise evaluation of the CTA bridge

Once the ratio of the peak value at the bump to the flat level in the lower frequency range is given by the curve-fitting or white-noise injection method, it is possible to estimate and then eliminate the inherent electric noise from the spectral components acquired. The black curve in figure 7 depicts the power spectrum of the CTA output at $U = 20$ m s^{-1} in practical use when $e_t = 0$. Frequency components lower than 1 kHz are due to residual turbulence in the free-stream mentioned before, while a bump peaking at 25–30 kHz is ascribed mainly to inherent electric noise of the CTA servo amplifier. Thus, the noise in the servo amplifier is found to behave like the white-noise injection into the bridge.

Assuming that this bump is due to the servo-amplifier noise, independent of velocity fluctuations, the electric noise below $f \approx 1$ kHz hidden in the residual turbulence can be estimated and thus eliminated easily. The green curve in figure 7 is representative of the CTA noise characteristic estimated by equation (8), with the input noise e_t given by the datasheet of the present servo amplifier shown in figure 8. The red dashed curve shows the power spectrum of actual residual turbulence when

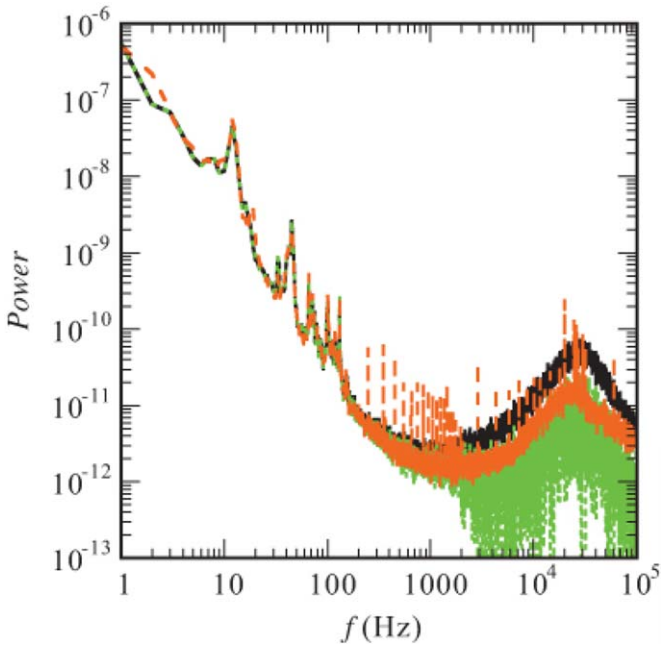

Figure 9. A comparison of the power spectra of free-stream turbulence at $U = 8$ m s^{-1}, measured using the present CTA (black solid line) and a commercially available low-noise CTA (Dantec Stramline Pro, orange broken line). The corrected spectrum for the present CTA using equation (8) is displayed in the green dotted line.

the servo-amplifier noise was thus eliminated, indicating that the overlap region (at around 1 kHz) between the electric noise and the residual turbulence can extend up to 3–4 kHz. In addition, the dynamic range of the CTA bridge was expanded by one order of magnitude.

We should also point out that spiky noise components appearing in the frequency range above 1 kHz were extremely weak, indicating that the electromagnetic shielding in the present small CTA system worked well, as expected. Consequently, the electric noise levels of the free-stream velocity of 20 m s^{-1} in the frequency range of 1 Hz to 1 kHz and 1 Hz to 250 kHz were 0.0025% and 0.07%, respectively.

Finally, to confirm that the present CTA system is robust to ambient electromagnetic noise, the power spectra of free-stream turbulence were compared with a commercially available low-noise CTA (Dantec Streamline Pro) at $U = 8$ m s^{-1} in figure 9. Here, residual turbulence in the wind tunnel was negligibly small for $f \geq 1$ kHz. The comparison shows that the power spectrum obtained with the present CTA did not include any line spectra corresponding to electric noise components, while they appeared for $f \geq 200$ Hz in the measurement by the conventional CTA. Thus, the shielding to electromagnetic noise worked quite well in the present compact CTA system, as expected. On the other hand, broadband noise for $f \geq 1$ kHz was slightly larger than the conventional CTA. However, such broadband noise, depending on the characteristics of the servo amplifier used, can be removed in the present CTA using the established transfer function equation (8). The corrected spectrum is also plotted in the figure for comparison, showing that the magnitude of broadband noise (above 1 kHz) was reduced to that for the Dantec CTA.

5. Conclusions

To improve the S/N ratio in CTA measurements, a compact low-noise CTA system was newly developed and its performance was investigated in detail. Special attention was paid to shortening the sensor-cable, which minimized cable reactance, maximized the electromagnetic shielding effect and simplified the transfer function. White noise and a square wave were used to examine the dynamic responses of the CTA. The results showed that the response waveform to the square-wave input was well reproduced by the theoretical response model to the step-function input. Three parameters in the transfer function, the damping coefficient ζ, the resonance frequency ω_r of the circuit and the thermal time constant M of the hot-wire sensor, were successfully determined by the curve-fitting method, and their variations in response to the flow velocity U were presented.

The results for the responses to a white-noise input demonstrated clearly that the transfer function with experimentally determined parameters described the CTA responses quite well over a wide frequency range; that is, between 1 Hz to 250 kHz in the present experiment. When the electric noise was assumed to be independent of velocity fluctuations, the transfer function allowed us to remove electric noise components from the acquired data, compensating the spectra of velocity fluctuations, beyond the resonant frequency of the CTA. By applying the established transfer function to the actual measurement, both the S/N ratio and the frequency range of the measurement could be improved significantly.

Acknowledgments

This work was supported by the JSPS Grant-in-Aid for Scientific Research (Grant No. 17K18939).

ORCID iDs

Ayumu Inasawa https://orcid.org/0000-0002-9695-8453
Shohei Takagi https://orcid.org/0000-0003-3361-7915
Masahito Asai https://orcid.org/0000-0002-5232-191X

References

[1] Perry A E 1982 *Hot-Wire Anemometry* (Oxford: Clarendon)
[2] Bruun H H 1995 *Hot-Wire Anemometry* (Oxford: Oxford University Press)
[3] Asai M, Inasawa A, Konishi Y, Hoshino S and Takagi S 2011 Experimental study on the instability of wake of axisymmetric streamlined body *J. Fluid Mech.* **675** 574–95
[4] Inasawa A, Floryan J M and Asai M 2014 Flow recovery downstream from a surface protuberance *Theor. Comput. Fluid Dyn.* **28** 427–47
[5] Imayama S, Alfredsson P H and Lingwood R J 2016 Experimental study of rotating-disk boundary-layer flow with surface roughness *J. Fluid Mech.* **786** 5–28
[6] Lysenko V I, Gaponov S A, Smorodsky B V, Yermolaev Y G, Kosinov A and Semionov N 2016 Combinedinfluence

of coating permeability and roughness on supersonic boundary layer stability and transition *J. Fluid Mech.* **798** 751–73
[7] Örlü R, Fransson H M and Alfredsson P H 2010 On near wall measurements of wall bounded flows–the necessity of an accurate determination of the wall position *Prog. Aerosp. Sci.* **46** 353–87
[8] Smits A J 2011 High-Reynolds number wall turbulence *Annu. Rev. Fluid Mech.* **43** 353–75
[9] Rodriguez-Lopez E, Bruce P J K and Buxton O R H 2015 A robust post-processing method to determine skin friction in turbulent boundary layers from the velocity profile *Exp. Fluids* **56** 68
[10] Vila C S, Vinuesa R, Ianiro A, Schlatter P and Örlü R 2017 On the identification of well-behaved turbulent boundary layers *J. Fluid Mech.* **822** 109–38
[11] Freymuth P 1968 Noise in hot-wire anemometers *Rev. Sci. Instrum.* **39** 550–7
[12] Örlü R, Alfredsson P H 2010 On spatial resolution issues related to time-averaged quantities using hot-wire anemometry *Exp. Fluids* **49** 101–10
[13] Chin C, Hutchins N, Ooi A and Marusic I 2011 Spatial resolution correction for hot-wire anemometry in wall turbulence *Exp. Fluids* **50** 1443–53
[14] Hutchins N, Monty J P, Hultmark M and Smits 2015 A direct measure of the frequency response of hot-wire anemometers: temporal resolution issues in wall-bounded turbulence *Exp. Fluids* **56** 18
[15] Ashok A, Bailey S, Hultmark M and Smits A 2012 Hot-wire spatial resolution effects in measurements of grid-generated turbulence *Exp. Fluids* **53** 1713–22
[16] Wood N B 1975 A method for determination and control of the frequency response of the constant-temperature hot-wire anemometer *J. Fluid Mech.* **67** 759–86
[17] Freymuth P 1977 Frequency response and electronic testing for constant-temperature anemometers *J. Phys. E: Sci. Instrum.* **10** 705–10
[18] Freymuth P 1997 Frequency response and electronic testing for constant-temperature anemometers *Meas. Sci. Technol.* **8** 174–7
[19] Weidman P D, Browand F K 1975 Analysis of a simple circuit for constant temperature anemometry *J. Phys. E: Sci. Instrum.* **8** 553–60
[20] Itsweire E C, Helland K N 1983 A high-performance low-cost constant-temperature hot-wire anemometer *J. Phys. E: Sci. Instrum.* **16** 549–53
[21] Analog Devices 2020 LT6200/LT6200-5/LT6200-10/LT6201 *Data Sheet*